

Supporting Information

**Eco-friendly, solution-processable and efficient low-energy lighting
phosphors: copper halide based hybrid semiconductors Cu₄X₆(L)₂ (X = Br, I)
composed of covalent, ionic and coordinate bonds**

Xiuze Hei,^a Simon J. Teat,^b Wei Liu,^a Jing Li*,^a

^a Department of Chemistry and Chemical Biology, Rutgers University, 123 Bevier Road,
Piscataway, NJ, 08854, USA

^b Advanced Light Source, Lawrence Berkeley National Laboratory, Berkeley, CA 94720, USA

TABLE OF CONTENT

S1. ^1H NMR spectroscopic data

S2. Structural plots and crystal images of compounds **1-4**

S3. DFT calculation details

S4. References

S1. ^1H NMR spectroscopic data

All ^1H NMR spectra data were collected using dimethyl sulfoxide-d6 as solvent. The peaks at 2.50 ppm and ~3.3 ppm are the residue DMSO and water peaks, respectively.

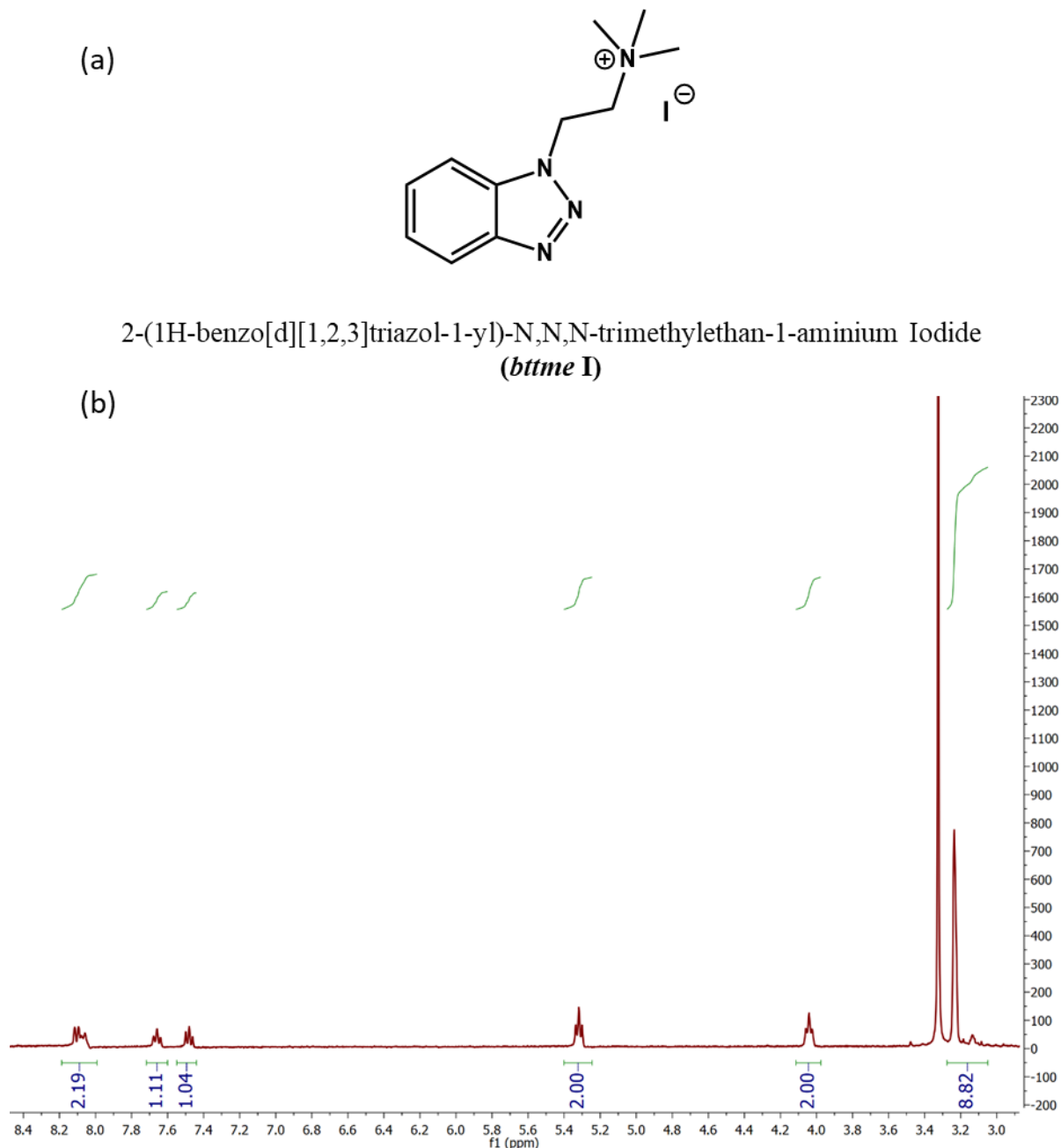
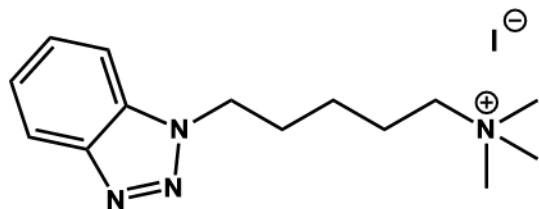


Figure S1. Structure and ^1H NMR spectrum of *btmse I*.

(a)



5-(1H-benzo[d][1,2,3]triazol-1-yl)-N,N,N-trimethylpentan-1-aminium Iodide
(bttmpe I)

(b)

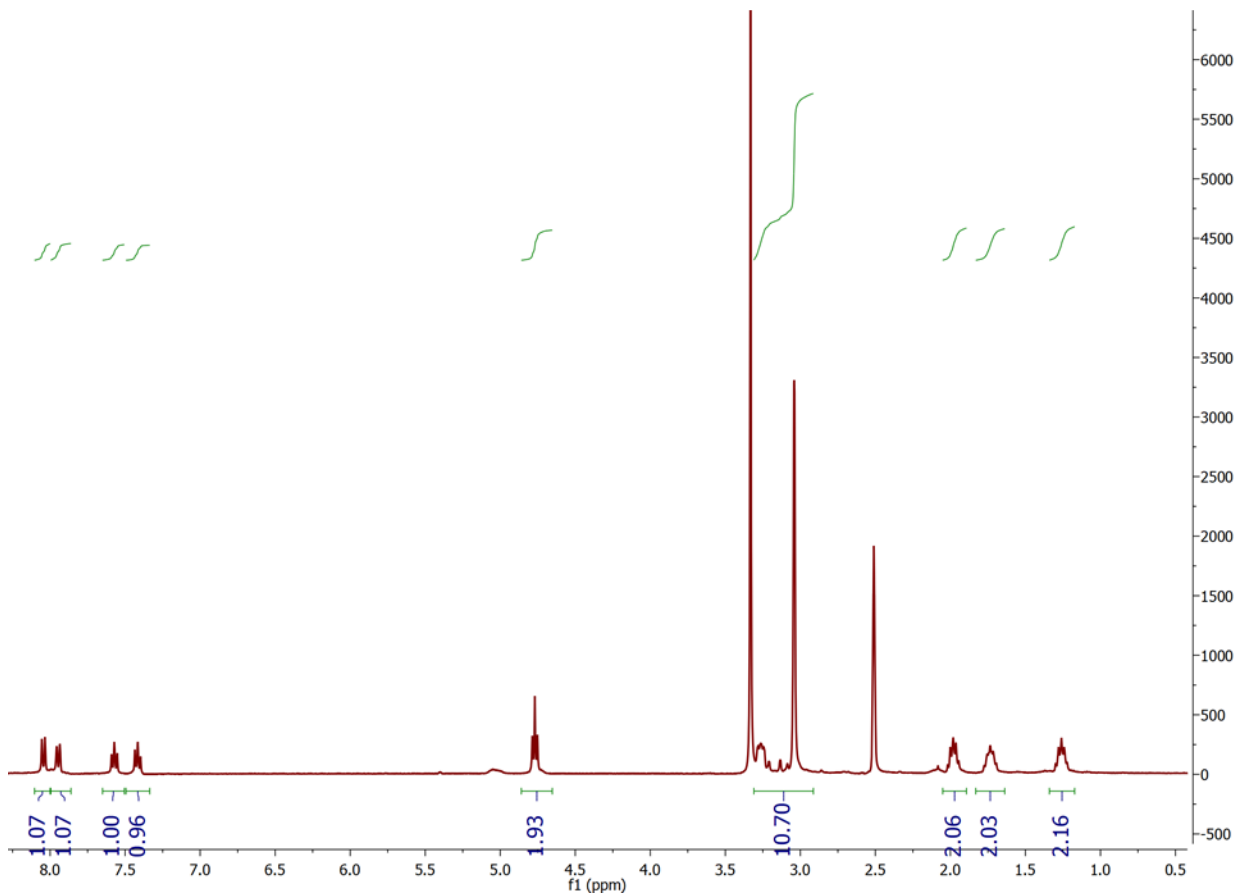


Figure S2. Structure and ^1H NMR spectrum of *bttmpe I*.

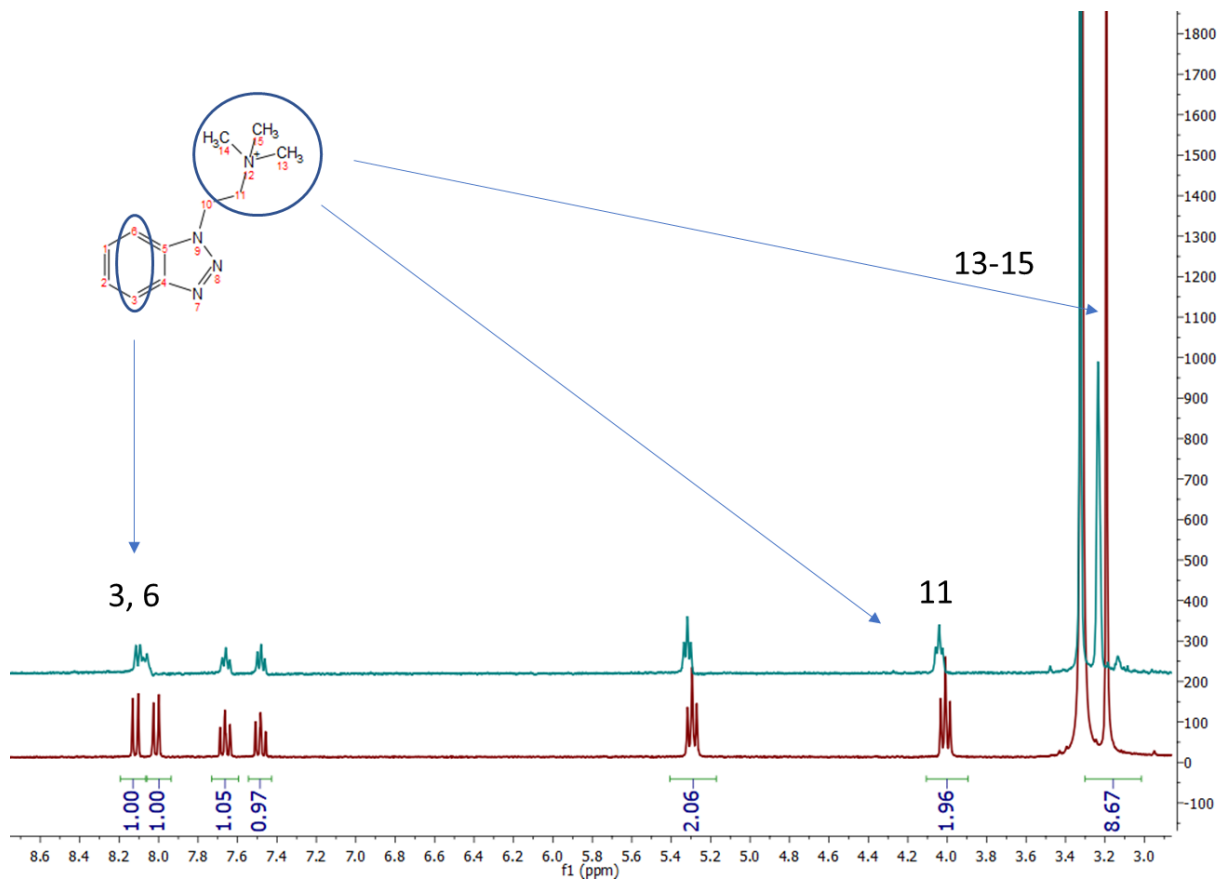


Figure S3. ¹H NMR spectra of dissolved compound **2** (bottom marron line) and free ligand *btme* I (top green line).

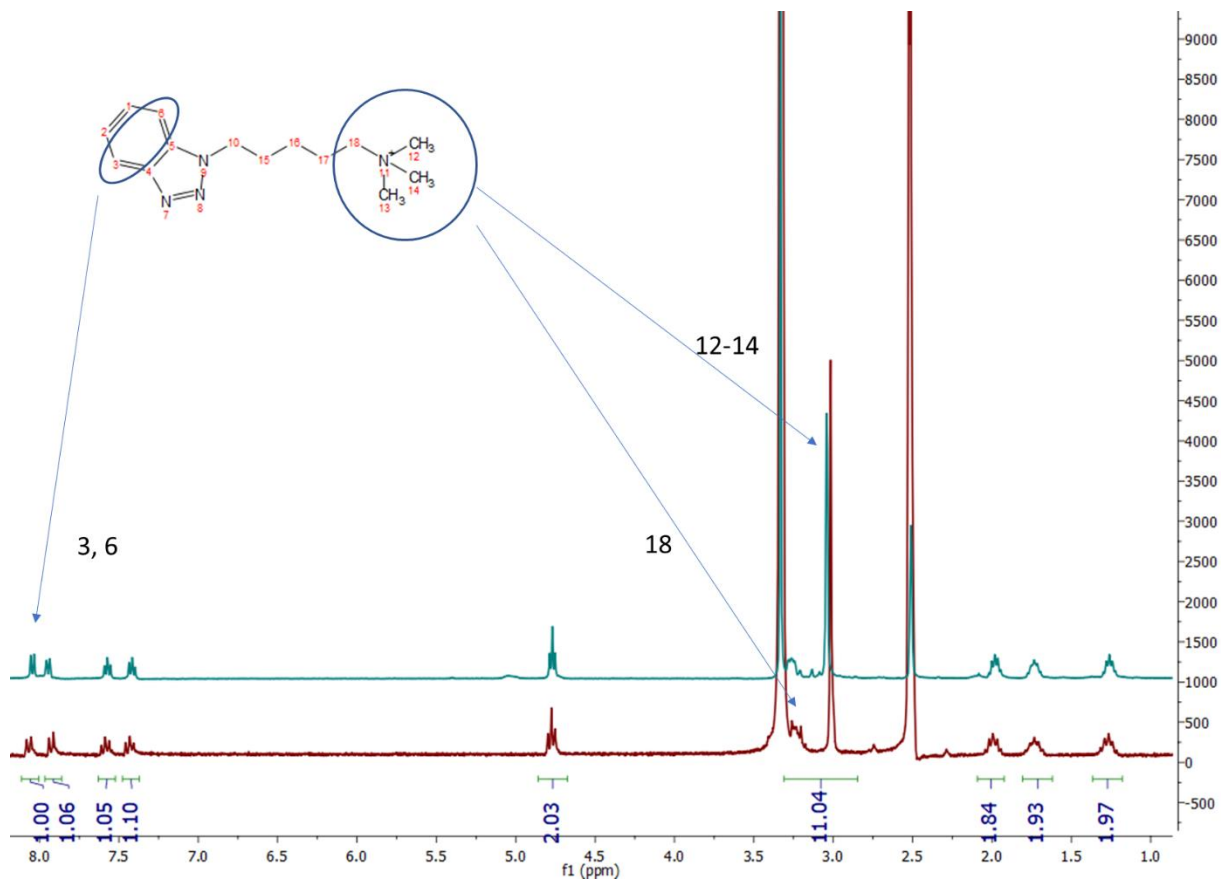


Figure S4. ^1H NMR spectra of dissolved compound **4** (bottom, marron) and free ligand *bttmpe* I (top, green).

S2. Structures, crystal images and optical absorption spectra of compounds 1-4.

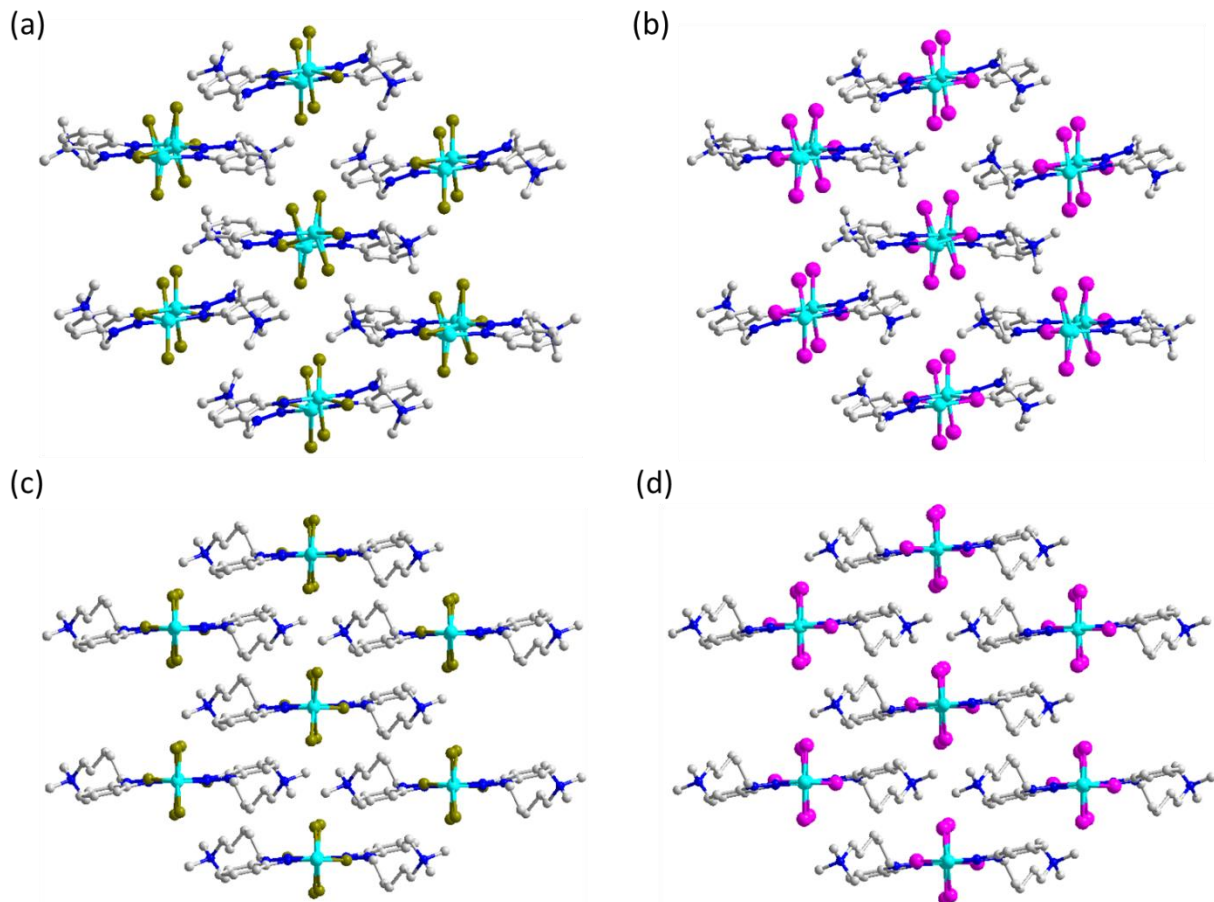


Figure S5. View of crystal structures along the chain direction. (a) **1**, (b) **2**, (c) **3** and (d) **4**.

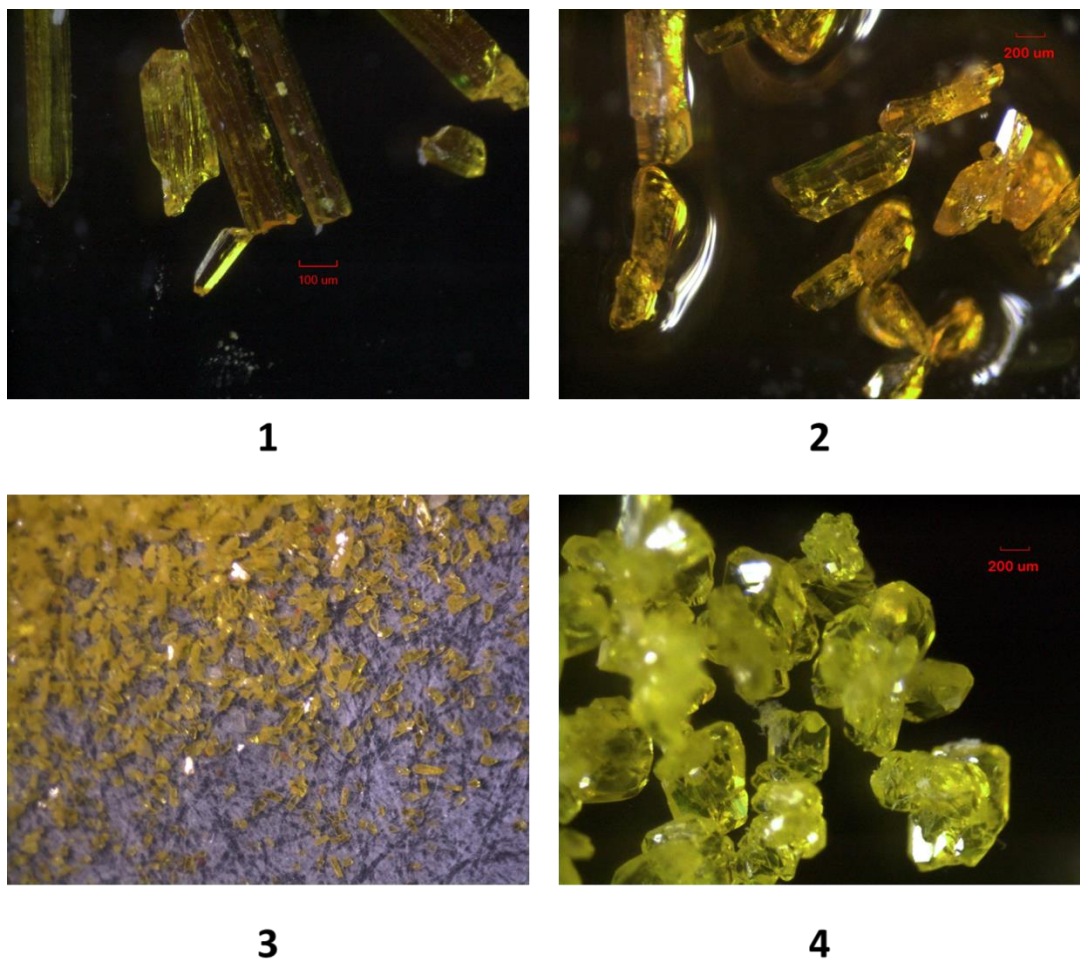


Figure S6. Optical images of single crystals of compounds **1-4**.

S3. DFT calculation details

(a) Electronic structure calculation details: Band gaps and density of states of selected compounds were calculated using the Cambridge Serial Total Energy Package (CASTEP) in Materials studio package¹ using the crystal structures obtained from single crystal X-ray analysis. Generalized gradient approximations (GGA) with Perdew-Burke-Ernzerhof (PBE) exchange-correlation functional (xc) were used for all calculations.² The plane-wave kinetic energy cutoff was set as 351 eV, ultrasoft pseudopotentials were used for all chemical elements and the total energy tolerance was set to be 2×10^{-5} eV/atom.

Table S1. Calculated compositions of VBM and CBM in compounds **1-4**.

		Cu	X	N & C
<i>Cu₄Br₆(btme)₂</i> (1)	VBM (%)	84.4	12.4	3.1
	CBM (%)	7.1	2.2	88.3
	Difference (%)	77	10	-85
<i>Cu₄I₆(btme)₂</i> (2)	VBM (%)	77.4	19.4	3.0
	CBM (%)	5.9	2.5	89.2
	Difference (%)	72	17	-86
<i>Cu₄Br₆(btmpe)₂</i> (3)	VBM (%)	85.2	11.6	3.0
	CBM (%)	6.5	1.7	89.2
	Difference (%)	79	10	-86
<i>Cu₄I₆(btmpe)₂</i> (4)	VBM (%)	78.1	18.6	3.0
	CBM (%)	5.4	2.1	90.0
	Difference (%)	73	16	-87

The percentage contributions were calculated by integrating the PDOS plots. VBM is the highest occupied band and CBM is the lowest unoccupied band.

Table S2. Summary of DFT calculation results.

Compound	Main contribution of atomic states in VBM	Main contribution of atomic states in CBM	MLCT (%)	XLCT (%)
Cu ₄ Br ₆ (<i>bttme</i>) ₂ (11)	Cu 3d, I 5p or Br 4p	C 2p and N 2p	77	10
Cu ₄ I ₆ (<i>bttme</i>) ₂ (2)			72	17
Cu ₄ Br ₆ (<i>bttmpe</i>) ₂ (3)			79	10
Cu ₄ I ₆ (<i>bttmpe</i>) ₂ (4)			73	16

MLCT: Metal to ligand charge transfer. XLCT: Halogen to ligand charge transfer.

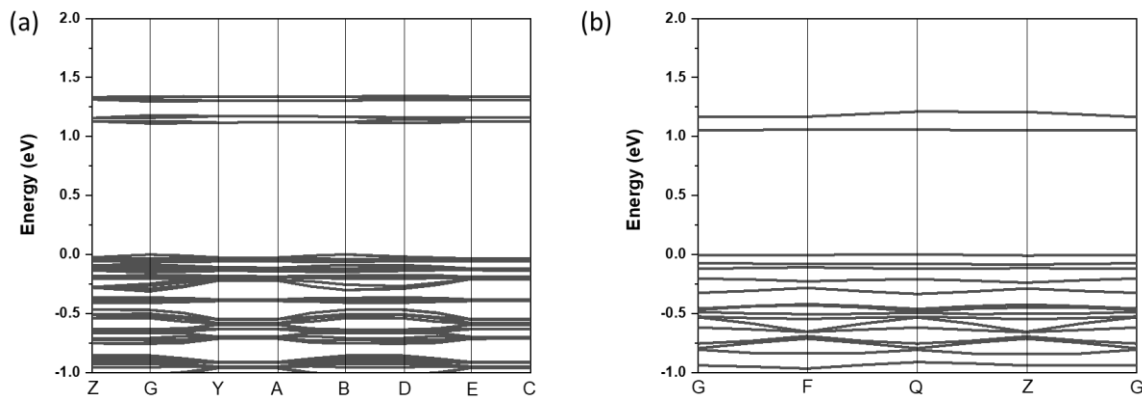


Figure S7. Band structures of compounds (a) **1** and (b) **3**.

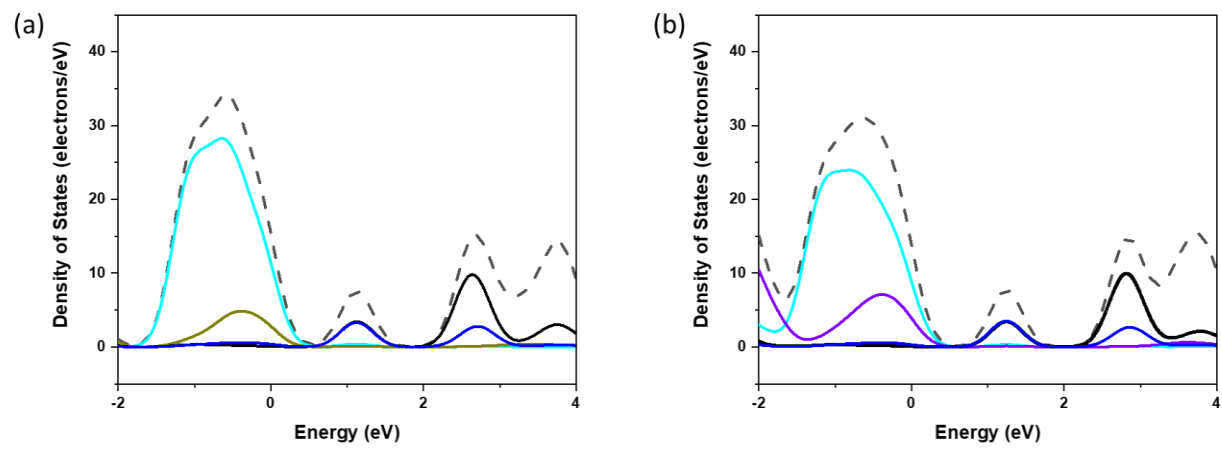


Figure S8. Total density of states (DOS) and projected density of states (PDOS) for compounds (a) **3** and (b) **4**.

(b) pKa calculation details: $G_{aq}^0(A)$ and $G_{aq}^0(HA^+)$ for each structure at N1 and N2 site were performed using density functional theory (B3LYP/6-31+G(d)) as implemented in Gaussian 16.³ All the geometries were fully optimized and calculated under SMD model using water as solvent. The temperature for the calculations was set to be 298 K.⁴

$$pK_a = \frac{\Delta G^0}{2.303RT}$$

$$pK_b = 14 - pK_a$$

$$\Delta G^0(HA^+) = G_g^0(A) + G_g^0(H^+) - G_g^0(HA^+) + \Delta G_{sol}^0(A) + \Delta G_{sol}^0(H^+) - \Delta G_{sol}^0(HA^+),$$

Where,

$$\Delta G_{sol}^0(A) = G_{aq}^0(A) - G_g^0(A)$$

$$\Delta G_{sol}^0(HA^+) = G_{aq}^0(HA^+) - G_g^0(HA^+)$$

$$\Delta G^0(HA^+) = G_g^0(H^+) + G_{aq}^0(A) + \Delta G_{sol}^0(H^+) - G_{aq}^0(HA^+)$$

Where,

$$G_g^0(H^+) = -6.28 \text{ kcal/mol}$$

$$\Delta G_{sol}^0(H^+) = -265.6 \pm 1 \text{ kcal/mol}$$

Table S3. Calculated pK_a and pK_b values of N1 and N2 of the ligands.

Ligand	# of carbon in the alkyl chain of the ligand (n)	pK _a of N1	pK _b of N1	pK _a of N2	pK _b of N2
bttme	2	-11.91896	25. 91896	-5.50168	19. 50168
bttmpe	5	-9.99068	23.99068	-3.28723	17.28723

(c) Calculation details for HOMO and LUMO energies of ligands: Density functional theory (DFT) calculations were applied to the neutral precursors of all cationic ligands by deducting an alkyl group from the quaternary nitrogen. All the calculations were performed by Gaussian 09⁵ with B3LYP hybrid functional and 6-31+G(d) basis set. A frequency calculation was always performed after geometry optimization of all ligand molecules to confirm that the calculations resulted in a true minimum.

Table S4. Calculated HOMO and LUMO energies of ligands.

Full Name	Abbrev	HOMO (eV)	LUMO (eV)
2-(1H-benzo[d][1,2,3]triazol-1-yl)-N,N,N-trimethylethan-1-aminium	<i>bttme</i>	-6.3672	-1.4708
5-(1H-benzo[d][1,2,3]triazol-1-yl)-N,N,N-trimethylpentan-1-aminium	<i>bttmpe</i>	-6.1171	-1.4123

S4. References

1. J. C. Stewart, D. S. Matthew, J. P. Chris, J. H. Phil, I. J. P. Matt, R. Keith and C. P. Mike, *Zeitschrift für Kristallographie - Crystalline Materials*, 2005, **220**, 567-570.
2. F. Lin, W. Liu, H. Wang and J. Li, *Chemical Communications*, 2020, **56**, 1481-1484.
3. M. J. Frisch, G. W. Trucks, H. B. Schlegel, G. E. Scuseria, M. A. Robb, J. R. Cheeseman, G. Scalmani, V. Barone, G. A. Petersson, H. Nakatsuji, X. Li, M. Caricato, A. V. Marenich, J. Bloino, B. G. Janesko, R. Gomperts, B. Mennucci, H. P. Hratchian, J. V. Ortiz, A. F. Izmaylov, J. L. Sonnenberg, Williams, F. Ding, F. Lipparini, F. Egidi, J. Goings, B. Peng, A. Petrone, T. Henderson, D. Ranasinghe, V. G. Zakrzewski, J. Gao, N. Rega, G. Zheng, W. Liang, M. Hada, M. Ehara, K. Toyota, R. Fukuda, J. Hasegawa, M. Ishida, T. Nakajima, Y. Honda, O. Kitao, H. Nakai, T. Vreven, K. Throssell, J. A. Montgomery Jr., J. E. Peralta, F. Ogliaro, M. J. Bearpark, J. J. Heyd, E. N. Brothers, K. N. Kudin, V. N. Staroverov, T. A. Keith, R. Kobayashi, J. Normand, K. Raghavachari, A. P. Rendell, J. C. Burant, S. S. Iyengar, J. Tomasi, M. Cossi, J. M. Millam, M. Klene, C. Adamo, R. Cammi, J. W. Ochterski, R. L. Martin, K. Morokuma, O. Farkas, J. B. Foresman and D. J. Fox, *Journal*, 2016.
4. Y. Niu and J. K. Lee, in *Applied Theoretical Organic Chemistry*, WORLD SCIENTIFIC (EUROPE), 2017, pp. 503-518.
5. M. J. Frisch, G. W. Trucks, H. B. Schlegel, G. E. Scuseria, M. A. Robb, J. R. Cheeseman, G. Scalmani, V. Barone, G. A. Petersson, H. Nakatsuji, X. Li, M. Caricato, A. V. Marenich, J. Bloino, B. G. Janesko, R. Gomperts, B. Mennucci, H. P. Hratchian, J. V. Ortiz, A. F. Izmaylov, J. L. Sonnenberg, Williams, F. Ding, F. Lipparini, F. Egidi, J. Goings, B. Peng, A. Petrone, T. Henderson, D. Ranasinghe, V. G. Zakrzewski, J. Gao, N. Rega, G. Zheng, W. Liang, M. Hada, M. Ehara, K. Toyota, R. Fukuda, J. Hasegawa, M. Ishida, T. Nakajima, Y. Honda, O. Kitao, H. Nakai, T. Vreven, K. Throssell, J. A. Montgomery Jr., J. E. Peralta, F. Ogliaro, M. J. Bearpark, J. J. Heyd, E. N. Brothers, K. N. Kudin, V. N. Staroverov, T. A. Keith, R. Kobayashi, J. Normand, K. Raghavachari, A. P. Rendell, J. C. Burant, S. S. Iyengar, J. Tomasi, M. Cossi, J. M. Millam, M. Klene, C. Adamo, R. Cammi, J. W. Ochterski, R. L. Martin, K. Morokuma, O. Farkas, J. B. Foresman and D. J. Fox, *Journal*, 2016.